Journal of ELECTRONIC MATERIALS, Vol. 45, No. 11, 2016
DOI: 10.1007/s11664-016-4803-z

Effects of Aging Treatment on Mechanical Properties of Sn-58Bi Epoxy Solder on ENEPIG-Surface-Finished PCB

JUNGSOO KIM,[1] WOO-RAM MYUNG,[2] and SEUNG-BOO JUNG[1,3]

1.—School of Advanced Materials Science and Engineering, Sungkyunkwan University, Seobu-ro 2066, Jangan-gu, Suwon 440-746, South Korea. 2.—SKKU Advanced Institute of Nanotechnology (SAINT), Sungkyunkwan University, Seobu-ro 2066, Jangan-gu, Suwon 440-746, South Korea. 3.—e-mail: sbjung@skku.edu

The mechanical properties of Sn-58Bi epoxy solder were evaluated by low-speed shear testing as functions of aging time and temperature. To determine the effects of epoxy, the interfacial reaction and mechanical properties of both Sn-58Bi and Sn-58Bi epoxy solder were investigated after aging treatment. The chemical composition and growth kinetics of the intermetallic compound (IMC) formed at the interface between Sn-58Bi solder and electroless nickel electroless palladium immersion gold (ENEPIG) surface finish were analyzed. Sn-58Bi solder paste was applied by stencil-printing on flame retardant-4 substrate, then reflowed. Reflowed samples were aged at 85°C, 95°C, 105°C, and 115°C for up to 1000 h. $(Ni,Pd)_3Sn_4$ IMC formed between Sn-58Bi solder and ENEPIG surface finish after reflow. Ni_3Sn_4 and Ni_3P IMCs formed at the interface between $(Ni,Pd)_3Sn_4$ IMC and ENEPIG surface finish after aging at 115°C for 300 h. The overall IMC growth rate of Sn-58Bi solder joint was higher than that of Sn-58Bi epoxy solder joint during aging. The shear strength of Sn-58Bi epoxy solder was about 2.4 times higher than that of Sn-58Bi solder due to the blocking effect of epoxy, and the shear strength decreased with increasing aging time.

Key words: Solder, Sn-58Bi, epoxy, IMC, ENEPIG

INTRODUCTION

For several decades, eutectic Sn–Pb solders have been widely used in the electronics industry because of their low price, good wettability, good plasticity, electrical conductivity, good reliability, and high productivity.[1–7] However, use of Pb is prohibited by the Regulation of Certain Hazardous Substances (RoHS) and Waste Electrical and Electronic Equipment (WEEE) due to the environmental pollution by and toxicity of Pb.[8–11]

Therefore, many researchers have investigated Pb-free solders. Among these, the Sn-Ag-Cu solder family is considered one of the most favorable because of its comprehensive properties including thermal resistance, wetting, and high creep resistance.[12–20] However, the high liquidus temperature of Sn-Ag-Cu solder induces thermal damage to the substrate and degrades the reliability of other components in the package during the reflow process.[21,22] On the other hand, Sn-58Bi solder is suitable for temperature-sensitive processes due to its low liquidus point (138°C).[23–26] It can also prevent thermal shock damage to electronic packages due to thermal expansion mismatch.[27–29] In addition, it has good yield strength, creep resistance, and cost efficiency.[30] However, Sn-Bi solder has poor ductility.[31] To overcome the brittleness of Sn-Bi solder, we investigated epoxy-containing Sn-58Bi solder with electroless nickel immersion gold (ENIG) and electroless nickel electroless palladium immersion gold (ENEPIG) surface finishes. There have been many previous studies concerning interfacial reactions between Sn-58Bi solder and various substrates.[32–34] The relationship between the intermetallic compound (IMC) growth kinetics and the diffusion mechanism has been determined. Ni-based

(Received October 22, 2015; accepted July 12, 2016; published online July 28, 2016)

surface finish is suitable for Cu bond pads, acts as a diffusion barrier for Sn-rich solder joints, and offers good corrosion resistance, a very flat and fine lead pitch, good wettability, a maskless plating process, and strong adhesion.[35] However, the Au solution used in the immersion process results in galvanic hypercorrosion of the Ni–P layer, referred to as "black pad," leading to solder joint failure.[36] ENEPIG with addition of a Pd layer is believed to prevent corrosion of the underlying Ni(P) layer during immersion in Au solution and to provide good wettability and a low consumption rate.[37] However, there is limited information concerning interfacial reactions between Sn-58Bi solder and ENEPIG substrates. In this work we therefore used an ENEPIG surface finish, the widest-latitude surface finish used in many electronic products.[38,39]

We focused on the relationship between IMC growth and activation energy to investigate the interfacial reactions between Sn-58Bi solder and ENEPIG substrate after aging treatment. In addition, the mechanical properties of the Sn-58Bi and Sn-58Bi epoxy solders were evaluated by low-speed shear testing to investigate the effect of epoxy.

EXPERIMENTAL PROCEDURES

Sn-58Bi solder was formed on ENEPIG-surface-finished printed circuit board (PCB). The substrate was surface mount device (SMD)-type flame retardant 4 (FR-4). The size of the bonding pad opening was 200 μm. The ENEPIG surface finishes were composed of 5 μm Ni, 0.1 μm Pd(P) (with 6.5 wt.% to 9.0 wt.% P), coated with 0.08 μm Au. We used Sn-58Bi solder paste (TLF-401-11; Tamura Co., Japan) and Sn-58Bi epoxy solder paste (SAM10-401-27; Tamura Co., Japan). The Sn-58Bi solder paste included 9.4% flux and had viscosity of 210 Pa s. The Sn-58Bi epoxy solder paste included 14.7% flux with epoxy and had viscosity of 234 Pa s and liquidus point of about 139°C. We evaluated the thermal behavior of the Sn-58Bi and Sn-58Bi epoxy solder pastes using differential scanning calorimetry (DSC; Exstar 6000, Seiko Instruments, Japan) at heating rate of approximately 5°C/min. Solder paste was placed on the bonding pad using a stencil-printing method. The reflow process was performed with peak temperature of 190°C for 5 min using a reflow machine (RF-430-N2; Japan Pulse Laboratory Co. Ltd., Japan) with four heating zones. Figure 1 shows the reflow temperature profile. Samples were cooled at room temperature after the reflow process, then cleaned with deflux solution and alcohol to remove flux. The Sn-58Bi and Sn-58Bi epoxy solders were aged at 85°C, 95°C, 105°C, and 115°C for 100 h, 300 h, 500 h, and 1000 h, respectively. The interface of the solder joint was examined by scanning electron microscopy (SEM, S-3000H; Hitachi, Japan). The composition of the IMC formed at the solder joint was analyzed by electron probe microanalysis (EPMA, JXA-8500F; JEOL, Japan). The mechanical properties of the solder joints were evaluated using a low-speed shear tester (PTR-1000; Rhesca Co., Japan). Figure 2 shows a schematic of the low-speed shear test. The conditions employed for the shear test were shear height of 30 μm and shear speed of 200 μm/s, in compliance with Joint Electron Device Engineering Council (JEDEC) standard 22-B117A. After the low-speed shear test, the fracture surface was observed using SEM.

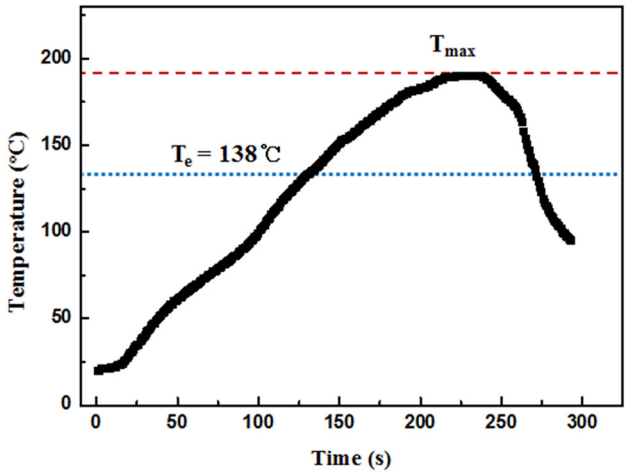

Fig. 1. Reflow temperature profile.

RESULTS AND DISCUSSION

Figures 3 and 4 show that the liquidus peak of the Sn-58Bi solder was around 140°C whereas that of the Sn-58Bi epoxy solder was around 139°C. It is important to note that the reaction of epoxy in the Sn-58Bi epoxy solder occurred at a liquidus point lower than the liquidus point of Sn-58Bi solder.

Figure 5 shows SEM micrographs of solder joints after the reflow process. Figure 5a and b shows 50° tilt views of Sn-58Bi and Sn-58Bi epoxy solders. Figure 5c and d shows cross-sectional micrographs of Sn-58Bi and Sn-58Bi epoxy solders. After reflow, the epoxy was filled around the Sn-58Bi solder, as shown in Fig. 5b and d.

Figure 6 shows cross-sectional SEM micrographs of Sn-58Bi and Sn-58Bi epoxy solder joints for different aging times and temperatures. Overall, the IMCs grew with increasing aging time and temperature for both solder types. Also, the IMC of the Sn-58Bi solder joints was slightly thicker than for the Sn-58Bi epoxy solder joints.

Figure 7 shows the IMC thickness of the Sn-58Bi and Sn-58Bi epoxy solders as a function of the square root of time for each aging temperature. The relationship between IMC thickness and aging time can be described by the equation

$$W = kt^n, \quad (1)$$

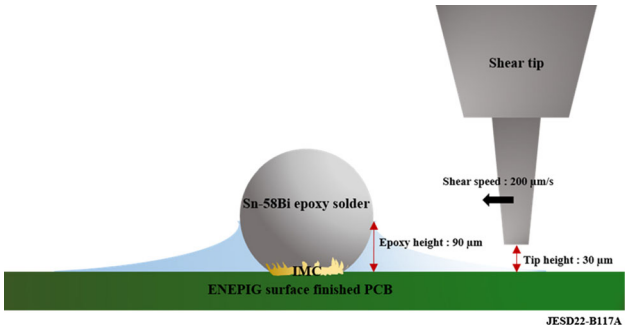

Fig. 2. Schematic of low-speed shear test.

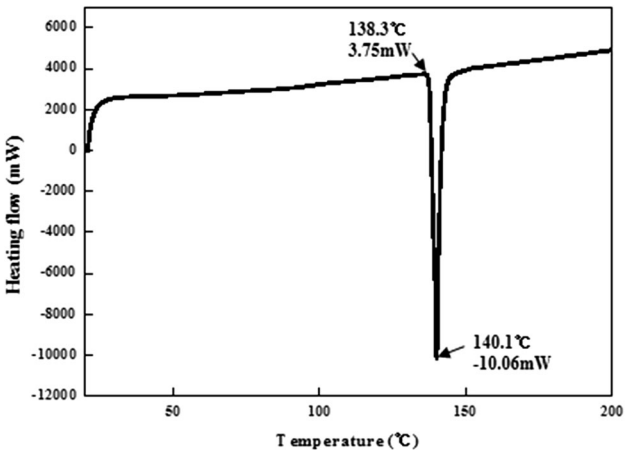

Fig. 3. DSC curve of Sn-58Bi solder paste with heating rate of 5°C/min.

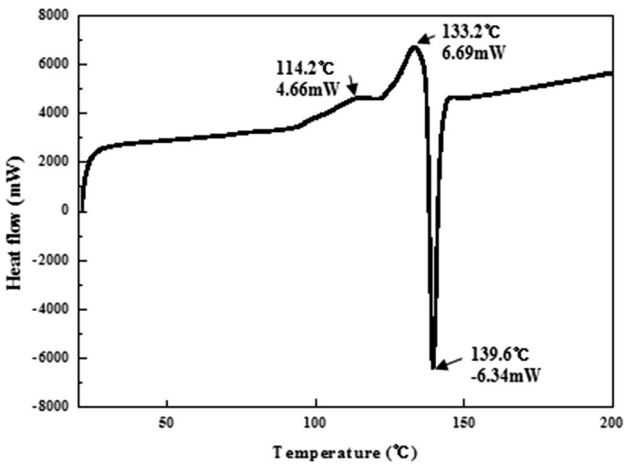

Fig. 4. DSC curve of Sn-58Bi epoxy solder paste with heating rate of 5°C/min.

where W is the reaction layer thickness, k is the growth rate constant, n is the time exponent, and t is the reaction time. The thickness of the IMC layer increased linearly with the square root of aging time. The IMC growth was faster for higher aging temperatures, especially 115°C. Table I presents the time exponent (n) and growth rate constant for the Sn-58Bi and Sn-58Bi epoxy solders. The value of the time exponent was approximately 0.5, and the IMC growth reaction was controlled by a diffusion mechanism.[40] The IMC growth rate for the Sn-58Bi solder was faster than for the Sn-58Bi epoxy solder.

To calculate the activation energy for IMC growth for the Sn-58Bi and Sn-58Bi epoxy solders, we used the Arrhenius equation

$$k^2 = k_0^2 \exp(-Q/RT), \tag{2}$$

where k^2 is the frequency factor, Q is the activation energy, R is the gas constant (8.314 J/mol K), and T is the aging temperature (K). The activation energy was calculated from the slope of the Arrhenius plot of $1/T$ versus $\ln k^2$. The growth rate k for the Sn-58Bi and Sn-58Bi epoxy solders is presented in Table II.

Figure 8 shows Arrhenius plots of $1/T$ versus $\ln k^2$ for the IMC with the Sn-58Bi and Sn-58Bi epoxy solder. In the case of Sn-58Bi solder, the 85°C to 95°C activation energy was 11.23 kJ/mol, and the 95°C to 115°C activation energy was 184.15 kJ/mol. In the case of Sn-58Bi epoxy solder, the 85°C to 95°C activation energy was 3.74 kJ/mol, and the 95°C to 115°C activation energy was 108.41 kJ/mol. The total activation energy for Sn-58Bi solder was 126.899 kJ/mol, whereas that for Sn-58Bi epoxy solder was 74.2 kJ/mol. In general, solder with high activation energy is expected to grow faster at higher temperature compared with solder with low activation energy. Also, there was a crossing point between the Sn-58Bi and Sn-58Bi epoxy solders at 85°C to 95°C because of their different activation energy values.

Figure 9 shows EPMA micrographs of the interface between the Sn-58Bi solder and ENEPIG surface finish depending on the aging time at 115°C. $(Ni,Pd)_3Sn_4$ IMC containing 3.05 at.% Au, 4.34 at.% Bi, and 1.83 at.% P formed at the interface between Sn-58Bi solder and ENEPIG surface finish after reflow. The chemical composition of this IMC was determined using energy-dispersive x-ray spectroscopy (EDX; Sn:Pd:Au:Bi:-Ni:P = 72.65:11.16:3.05:4.34:5.76:1.83, at.%). When aged for 300 h, Ni_3Sn_4 and Ni_3P IMCs formed under the $(Ni,Pd)_3Sn_4$ IMC. The Ni_3Sn_4 and Ni_3P IMCs contained 6 at.% Bi. The $(Ni,Pd)_3Sn_4$ and Ni_3Sn_4 IMCs grew continuously over 1000 h of aging. The Pd and Au in the IMC moved up with increasing aging time based on the mapping micrograph and quantitative analysis. A Bi-rich region remained on the IMC because Sn, Ni, Pd, and Au reacted to form an IMC. In addition, the Bi-rich phase and Sn-rich phase coarsened with aging treatment.

Figure 10 shows EPMA micrographs of the interface between Sn-58Bi epoxy solder and ENEPIG surface finish depending on the aging time at 115°C. In the Sn-58Bi epoxy solder, Pd and Au flakes were formed as reflowed. $(Ni,Pd)_3Sn_4$ IMC containing 8 at.% Bi and 5 at.% Au formed at 300 h. Ni_3Sn_4 and

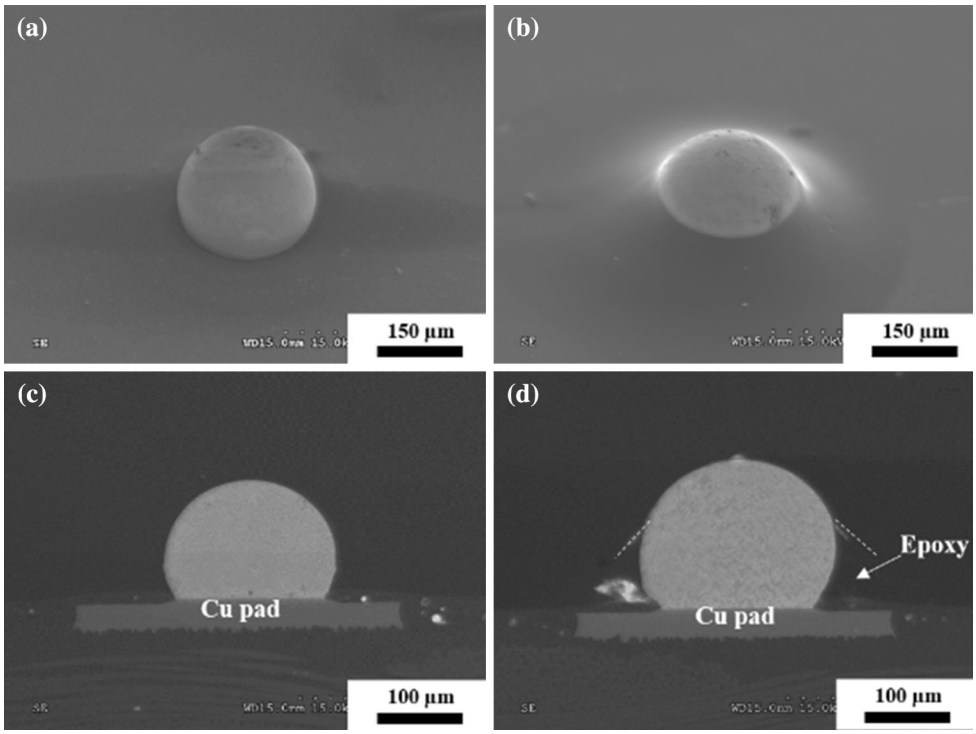

Fig. 5. SEM micrographs of solder joints after reflow: 50° tilt views of (a) Sn-58Bi and (b) Sn-58Bi epoxy solder; cross-sectional micrographs of (c) Sn-58Bi and (d) Sn-58Bi epoxy solder.

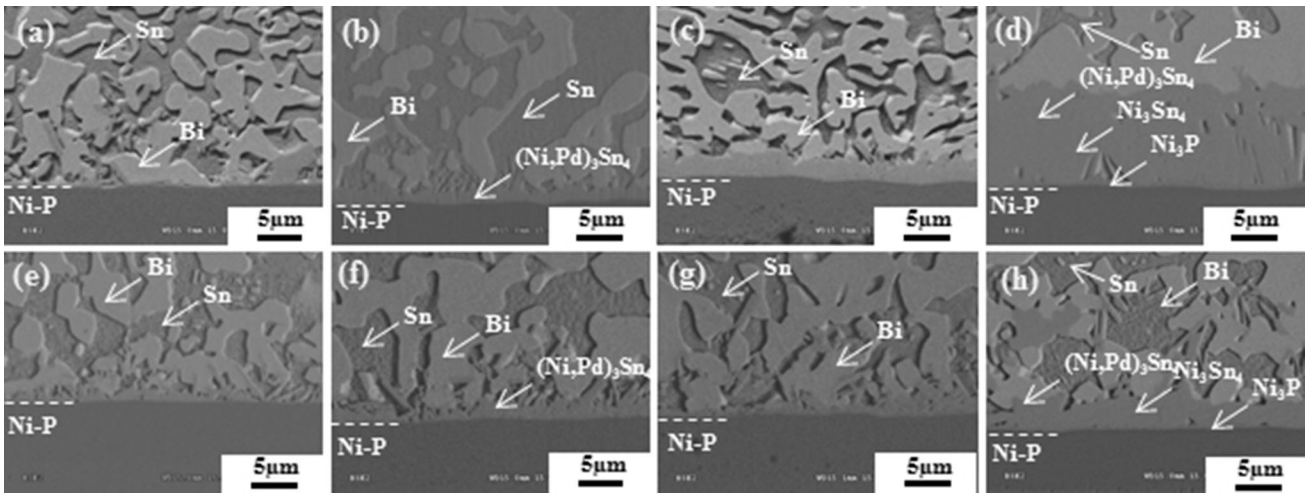

Fig. 6. Cross-sectional SEM micrographs of (a–d) Sn-58Bi and (e–h) Sn-58Bi epoxy solder joints after aging at (a, e) 85°C for 100 h, (b, f) 85°C for 1000 h, (c, g) 115°C for 100 h, and (d, h) 115°C for 1000 h.

Ni_3P IMCs containing 6 at.% Bi and 1.5 at.% Au formed between the $(Ni,Pd)_3Sn_4$ IMC and ENEPIG surface finish. At 1000 h of aging, $(Ni,Pd)_3Sn_4$ and Ni_3Sn_4 IMCs grew continuously. Regarding the total composition of the IMC, the amounts of Au, Pd, and Bi decreased and the Ni content increased with increasing aging time. Thus, Pd, Au, and Sn were the major reactants in reflow. The Ni(P) and Sn in the solder were the major reactants with increasing aging time. Although the Sn-58Bi epoxy solder did not demonstrate clearly different behavior from the Sn-58Bi solder, needle-type Pd and Au were present in vertical form in the IMC of the Sn-58Bi epoxy solder. We assumed that the epoxy in the Sn-58Bi epoxy solder affected the IMC thickness, although this requires further evaluation.

The shear strength of the Sn-58Bi solder including epoxy was evaluated by low-speed shear test, in compliance with JESD22-B117A. After reflow, the Sn-58Bi solder was encircled by epoxy approximately

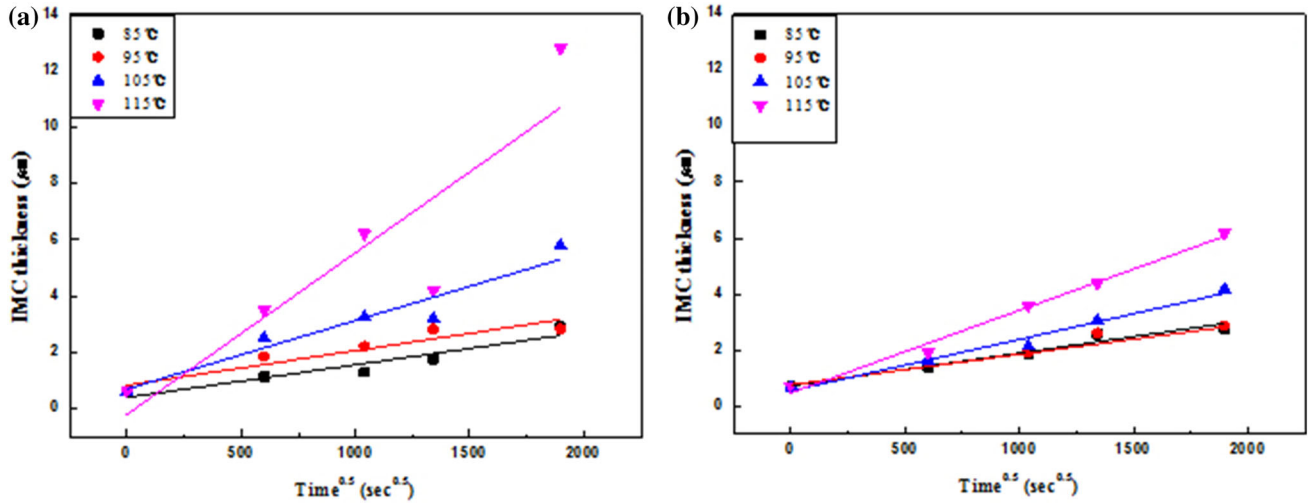

Fig. 7. IMC thickness as function of square root of time for each aging temperature for (a) Sn-58Bi and (b) Sn-58Bi epoxy solder.

Table I. Calculated growth rate constant and time exponent (n) as functions of aging temperature

Solder	Temperature (°C)	n	k^2 (10^{-15} cm^2/s)
Sn-58Bi solder	85	0.65	13.00
	95	0.27	14.40
	105	0.39	61.50
	115	0.53	321.49
Sn-58Bi epoxy solder	85	0.57	13.45
	95	0.41	13.92
	105	0.58	33.49
	115	0.65	87.03

Table II. Growth rate k for Sn-58Bi and Sn-58Bi epoxy solder

Solder	Temperature (°C)	k (μm/s)
Sn-58Bi solder	85	0.00114
	95	0.0012
	105	0.00248
	115	0.00567
Sn-58Bi epoxy solder	85	0.006
	95	0.00118
	105	0.00183
	115	0.00295

90 μm in height. During the shear test, the height of the tip of the shear tester from the substrate surface was 30 μm, as shown in Fig. 2. The tip of the shear tester collided with the epoxy surrounding the solder ball, about 60 μm. Fracture occurred in the epoxy and then propagated inside the solder ball. Shear strength–displacement (F–x) curves obtained from the shear test are shown in Fig. 11. The overall shape of the F–x curves changed with epoxy addition. The Sn-58Bi epoxy solder indicated greater elongation than the Sn-58Bi solder. However, the stress dropped sharply after peaking at the maximum shear strength for both solders. Thus, the shear strength of the Sn-58Bi epoxy solder was improved by the blocking effect of epoxy.[24] The shear strength of the Sn-58Bi epoxy solder was about 2.4 times higher than that of the Sn-58Bi solder.

Figure 12 shows the shear strength of the Sn-58Bi and Sn-58Bi epoxy solders as functions of aging time and temperature. The shear strength decreased with increasing aging time and temperature for both the Sn-58Bi and Sn-58Bi epoxy solders because of the increasing thickness and coarsening of the IMC.

Figure 13 shows the fracture energy of the Sn-58Bi and Sn-58Bi epoxy solders as a function of aging time and temperature after the low-speed shear test. The fracture energy of the Sn-58Bi epoxy solder was higher than that of the Sn-58Bi solder at all aging temperatures and times. The Sn-58Bi epoxy solder had high fracture energy because of the stress imparted by the epoxy around the solder. Also, the fracture energy of the solder tended to decrease with increasing aging time and temperature for both the Sn-58Bi and Sn-58Bi epoxy solders.

Figure 14 shows top-view micrographs of the Sn-58Bi and Sn-58Bi epoxy solders after low-speed shear test for various aging times at 115°C. Ductile fracture of the surface was observed in the Sn-58Bi and Sn-58Bi epoxy solder after reflow based on detection of Sn and Bi elements by EDX. The image in Fig. 14a also demonstrates ductile fracture. However, Fig. 14b–e and g–j shows brittle fracture surface for the Sn-58Bi and Sn-58Bi epoxy solders after aging treatment. Sn and Ni elements were

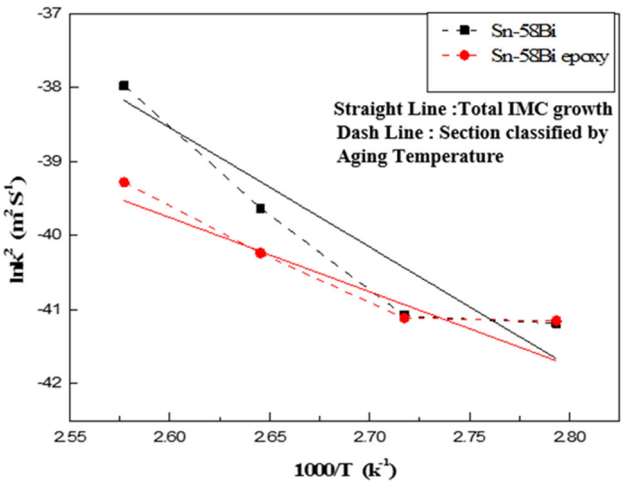

Fig. 8. Arrhenius plot for IMC layer growth.

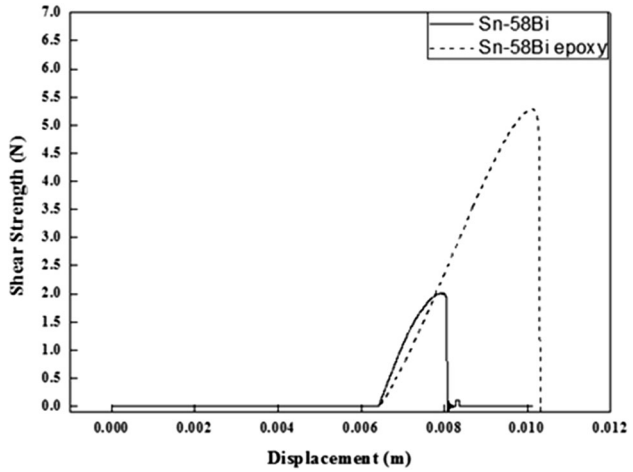

Fig. 11. *F–x* curves for Sn-58Bi and Sn-58Bi epoxy solders.

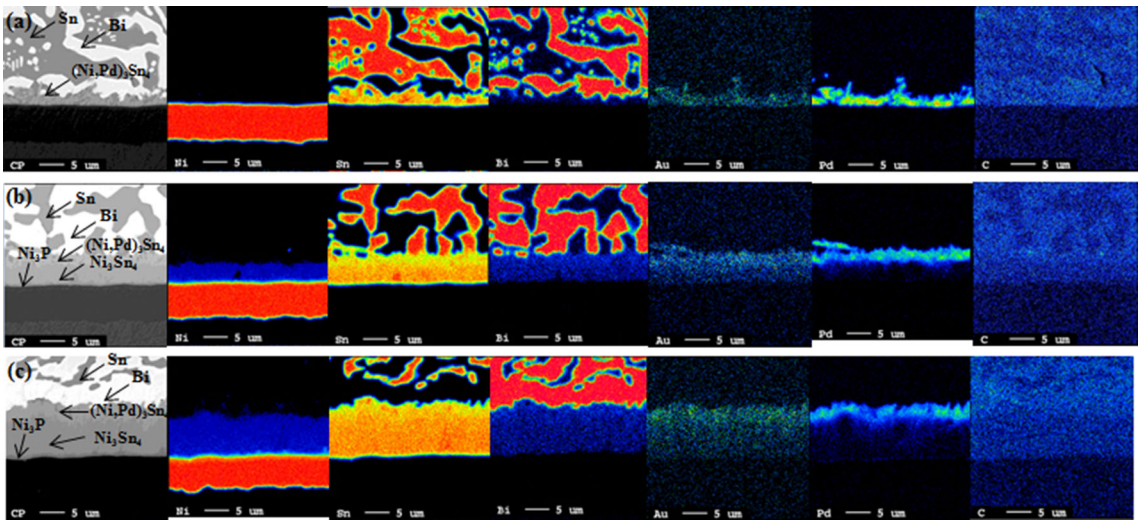

Fig. 9. EPMA mapping results of Sn-58Bi solder aged at 115°C: (a) as reflowed, (b) 300 h, (c) 1000 h.

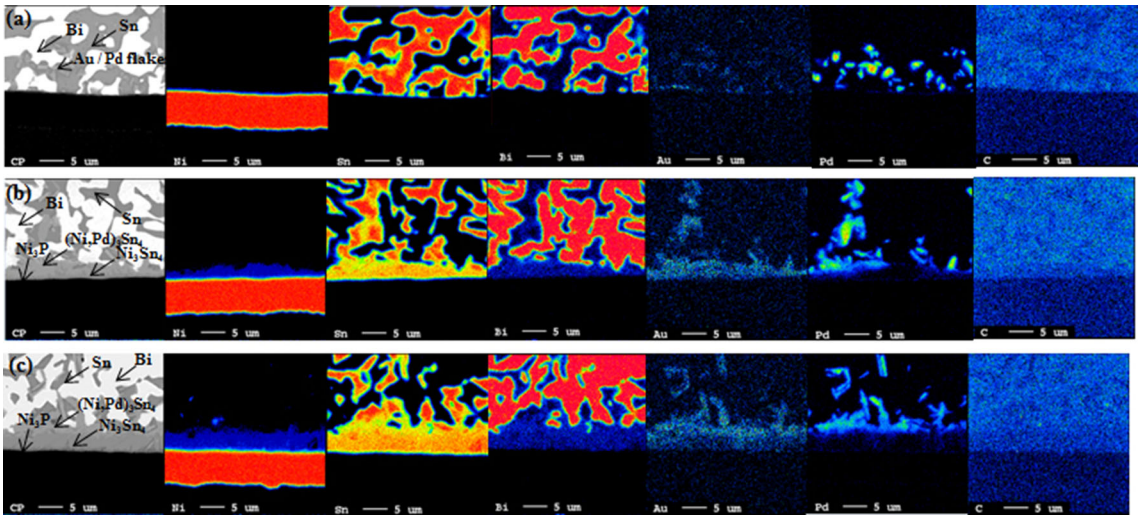

Fig. 10. EPMA mapping results of Sn-58Bi epoxy solder aged at 115°C: (a) as reflowed, (b) 300 h, (c) 1000 h.

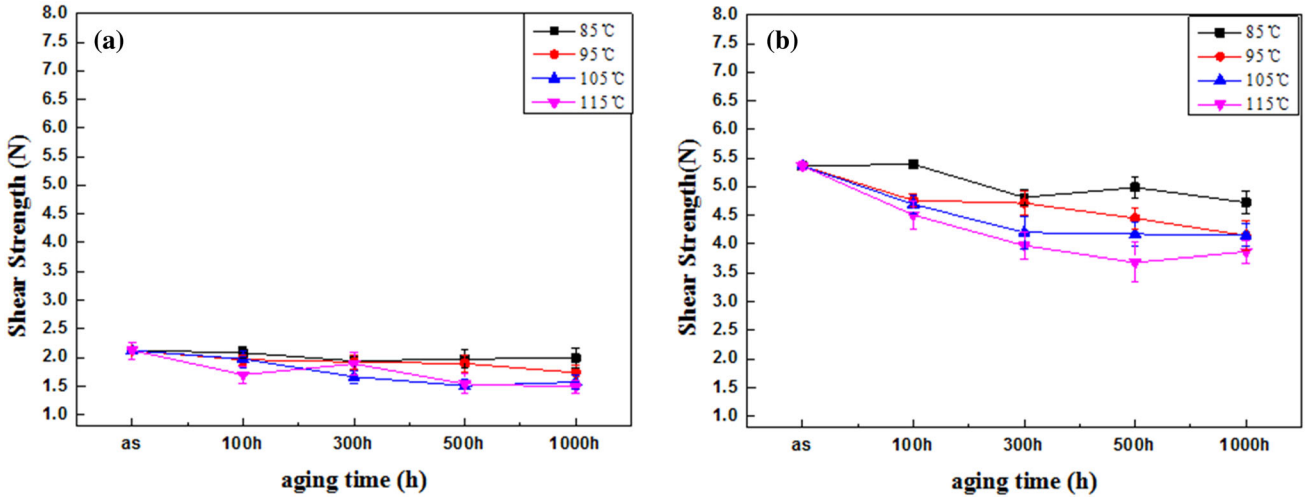

Fig. 12. Shear strength of solder joints as function of aging time and temperature for (a) Sn-58Bi and (b) Sn-58Bi epoxy solder.

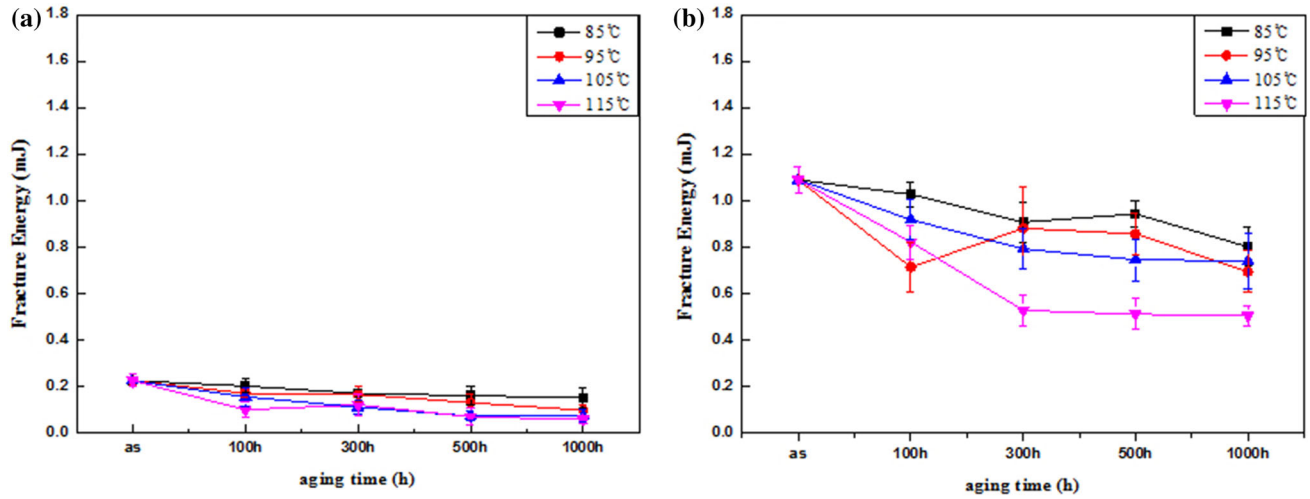

Fig. 13. Fracture energy of solder joints as function of aging time and temperature for (a) Sn-58Bi and (b) Sn-58Bi epoxy solder.

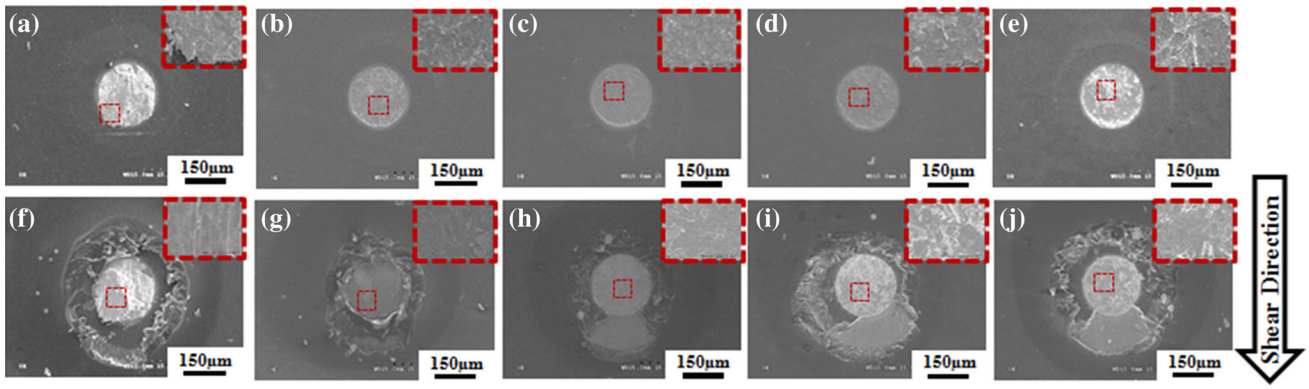

Fig. 14. Fracture surfaces of Sn-58Bi solder (a–e) and Sn-58Bi epoxy solder (f–j) after shear test: (a, f) as reflowed, and after aging at (b, g) 115°C for 100 h, (c, h) 115°C for 300 h, (d, i) 115°C for 500 h, and (e, j) 115°C for 1000 h.

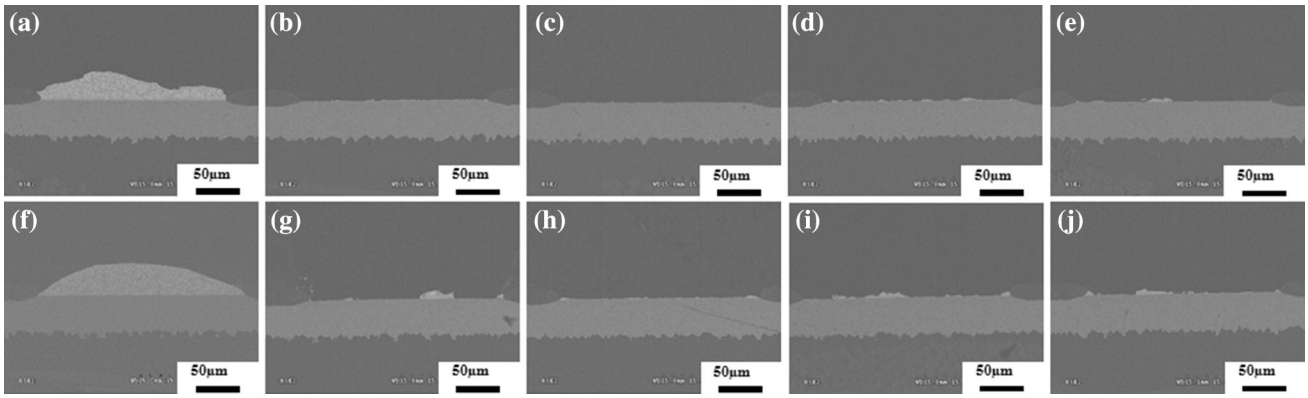

Fig. 15. Cross-sectional SEM micrographs of fracture surfaces of Sn-58Bi solder (a–e) and Sn-58Bi epoxy solder (f–j) after shear test: (a, f) as reflowed, and after aging at (b, g) 115°C for 100 h, (c, h) 115°C for 300 h, (d, i) 115°C for 500 h, and (e, j) 115°C for 1000 h.

detected by EDX. The composition of the IMC was Ni_3Sn_4.

Figure 15 shows cross-sectional SEM micrographs of fracture surfaces of Sn-58Bi and Sn-58Bi epoxy solder. Figure 15a and f shows that extra solder was observed on the surface for both solder types after reflow. However, Fig. 15b–e and g–j shows that extremely small amounts of solder remained on the surface.

CONCLUSIONS

We compared the interfacial reaction and mechanical properties for Sn-58Bi and Sn-58Bi epoxy solders with ENEPIG surface finish. A Sn-rich phase and Bi-rich phase of the eutectic group and a $(Ni,Pd)_3Sn_4$ IMC formed at the interface between Sn-58Bi solder and ENEPIG surface finish after reflow. Ni_3Sn_4 and Ni_3P IMCs formed between $(Ni,Pd)_3Sn_4$ and ENEPIG surface finish at 115°C after 300 h of aging. In addition, for both the Sn-58Bi and Sn-58Bi epoxy solder, the $(Ni,Pd)_3Sn_4$ and Ni_3Sn_4 IMCs increased with increasing aging time and temperature. The total IMC thickness was slightly thinner for the Sn-58Bi epoxy than the Sn-58Bi solder. The total IMC growth was controlled by a diffusion mechanism because the time exponent was approximately 0.5 for both solders. The activation energy of the Sn-58Bi epoxy solder was lower than that of the Sn-58Bi solder. The low-speed shear test results revealed that the Sn-58Bi epoxy solder had higher shear strength and fracture energy than the Sn-58Bi solder. Addition of epoxy to the Sn-58Bi solder improved its mechanical properties. Therefore, Sn-58Bi epoxy is fully expected to replace Sn-58Bi solder.

ACKNOWLEDGEMENT

This work was supported by the Human Resources Program in Energy Technology of the Korea Institute of Energy Technology Evaluation and Planning (KETEP) granted financial resource from the Ministry of Trade, Industry, and Energy, Republic of Korea (20154030200870).

REFERENCES

1. J.W. Yoon and S.B. Jung, *J. Alloys Compd.* 359, 202 (2003).
2. C. Kanchanomai, Y. Miyashita, and Y. Mutoh, *Int. J. Fatigue* 24, 987 (2002).
3. B.S. Chiou, K.C. Liu, J.G. Duh, and P.S. Palanisamy, *IEEE Comp. Hybr.* 13, 267 (1990).
4. Y. Zhang, Z. Cai, J.C. Suhling, P. Lall, and M.J. Bozack, in *2008 58th Electronic Components and Technology Conference* (IEEE, 2008), pp. 99–112.
5. C.E. Ho, R.Y. Tsai, Y.L. Lin, and C.R. Kao, *J. Electron. Mater.* 31, 584 (2002).
6. M. Amagai, M. Watanabe, M. Omiya, K. Kishimoto, and T. Shibuya, *Microelectron. Reliab.* 42, 951 (2002).
7. C.B. Lee, Y.E. Shin, C.C. Shur, and S.B. Jung, *Mater. Trans.* 42, 751 (2001).
8. J.W. Yoon, C.B. Lee, and S.B. Jung, *J. Electron. Mater.* 32, 1195 (2003).
9. J. Glazer, *J. Electron. Mater.* 23, 693 (1994).
10. J.W. Yoon, W.C. Moon, and S.B. Jung, *Microelectron. Eng.* 83, 2329 (2006).
11. K. Zeng and K.N. Tu, *Mater. Sci. Eng. A Struct.* 38, 55 (2002).
12. S.K. Kang, *J. Electron. Mater.* 23, 701 (1994).
13. C.B. Lee, J.W. Yoon, S.J. Suh, S.B. Jung, C.Y. Yang, C.C. Shur, and Y.E. Shin, *J. Mater. Sci.* 14, 487 (2003).
14. J.W. Yoon, S.W. Kim, J.M. Koo, D.G. Kim, and S.B. Jung, *J. Electron. Mater.* 33, 1190 (2004).
15. J.W. Yoon, S.W. Kim, and S.B. Jung, *J. Alloys Compd.* 392, 247 (2005).
16. K.S. Kim, S.H. Huh, and K. Suganuma, *Mater. Sci.* A333, 106 (2002).
17. J.W. Yoon, B.I. Noh, J.H. Yoon, H.B. Kang, and S.B. Jung, *J. Alloys Compd.* 509, L153 (2011).
18. I. Shohji, T. Yoshida, T. Takahashi, and S. Hioki, *J. Mater. Sci.* 15, 219 (2004).
19. J.W. Yoon, B.I. Noh, Y.H. Lee, H.S. Lee, and S.B. Jung, *Microelectron. Reliab.* 48, 1864 (2008).
20. S.Y. Chang, L.C. Tsao, M.W. Wu, and C.W. Chen, *J. Mater. Sci.: Mater. Electron.* 23, 100 (2012).
21. J.H. Kim, Y.C. Lee, S.M. Lee, and S.B. Jung, *Microelectron. Eng.* 120, 77 (2014).
22. J.W. Kim, D.G. Kim, J.M. Koo, J.W. Yoon, S. Choi, K.S. Kim, J.D. Nam, H.J. Lee, J. Joo, and S.B. Jung, *Mater. Trans.* 48, 1070 (2007).
23. J.W. Yoon, C.B. Lee, and S.B. Jung, *Mater. Trans.* 43, 1821 (2002).
24. W.R. Myung, Y.I. Kim, and S.B. Jung, *J. Alloys Compd.* 615, S411 (2014).
25. X. Gu, K.C. Yung, and Y.C. Chan, *J. Mater. Sci.: Mater. Electron.* 21, 1090 (2010).
26. J.S. Kim, W.R. Myung, and S.B. Jung, *J. Microelectron. Packag. Soc.* 21, 97 (2014).

27. C.C. Chi, L.C. Tsao, and T.H. Chuang, *J. Mater. Eng. Perform.* 17, 134 (2008).
28. H.W. Miao and J.G. Duh, *Mater. Chem. Phys.* 71, 255 (2001).
29. Z. Mei and J.W. Morris Jr., *J. Electron. Mater.* 21, 599 (1992).
30. H. Sun, Q. Li, and Y.C. Chan, *J. Mater. Sci.: Mater. Electron.* 25, 4380 (2014).
31. C. Fuchs, T. Schreck, and M. Kaloudis, *J. Mater. Sci.* 47, 4036 (2012).
32. P.T. Vianco, A.C. Kilgo, and R. Grant, *J. Electron. Mater.* 24, 1493 (1995).
33. C. Chen, C.E. Ho, A.H. Lin, G.L. Luo, and C.R. Kao, *J. Electron. Mater.* 29, 1200 (2000).
34. Y. Yen, D.W. Wen, K.-D. Liaw, and H. Chen. *J. Electron. Mater.* 39, 2412 (2010).
35. C.F. Tseng, T.K. Lee, G. Ramakrishna, K.C. Liu, and J.G. Duh, *Mater. Lett.* 65, 3216 (2011).
36. K. Zeng, R. Stierman, D. Abbot, and M. Murtuza, in *Thermal and Thermomechanical Proceedings 10th Intersociety Conference on Phenomena in Electronics Systems, 2006* (IEEE, 2006).
37. C.Y. Ho, J.G. Duh, C.W. Lin, C.J. Lin, Y.H. Wu, H.C. Hong, and T.H. Wang, *J. Mater. Sci.* 48, 2724 (2013).
38. G. Milad and M. Orduz, *Circuit World* 34, 25 (2007).
39. J.W. Yoon, B.I. Noh, and S.B. Jung, *J. Electron. Mater.* 40, 1950 (2011).
40. J.W. Yoon, C.B. Lee, and S.B. Jung, *Mater. Sci. Technol. Ser.* 19, 1101 (2003).